Phase behavior of semiflexible-coil diblock copolymers: a hybrid numerical SCFT approach

Wendi Song,[ab] Ping Tang,*[ab] Feng Qiu,[ab] Yuliang Yang[ab] and An-Chang Shi[ab]

The phase behavior of semiflexible-coil diblock copolymer melts is studied by solving the self-consistent field theory (SCFT) equations of wormlike chains. Significant improvement of numerical accuracy and stability is achieved by a hybrid numerical implementation of SCFT, in which the space-dependent functions are treated using a spectral method and the orientation-dependent functions are discretized on a unit sphere (3D Euclidean space) with an icosahedron triangular mesh. The angular Laplacian is solved in real-space using a finite volume algorithm. Phase diagrams of the model system are constructed from SCFT. Phase transitions between various smectic phases such as monolayer and bilayer smectic-A, monolayer and bilayer smectic-C, as well as folded smectic phases, are predicted. In particular, the stability of the monolayer and bilayer smectic phases is associated with the competition between interfacial energy and coil-stretching entropy, which strongly depends on the interplay between orientational interaction and microphase separation and the topological disparity between the semiflexible and coil blocks.

Introduction

Rod-coil block copolymers have attracted increasing recent attention because this class of polymers are essential in a wide range of applications[1] in areas such as organic electronics,[2] biotechnology, and high-performance resins. In these macromolecules, chain rigidity usually originates from π-conjugation, helical secondary structures or aromatic groups, leading to orientation order and liquid crystalline behavior. Compared with the classical coil-coil block copolymers, rod-coil block copolymers exhibit more complex phase behavior due to the coupling between microphase separation and liquid-crystalline ordering. A variety of rod-coil block copolymers have been experimentally observed to self-assemble into a series of novel structures, including layered smectics, arrowheads, wavy lamellae, zig-zags,[3,4] perforated lamellae[5] as well as folded helical peptides.[6–11] A generic observation is that, compared with corresponding coil-coil block copolymers, the liquid-crystalline interactions tend to stabilize planar interfaces, leading to a large lamellar region in the phase diagram.[12–16] On the other hand, exploring the whole phase space of rod-coil block copolymers presents a formidable task due to a large number of controlling parameters. For example, the rod and coil blocks have different scaling behaviors as a function of molecular weight N: the unperturbed coil size scales as $N^{1/2}$ whereas the rod block has a characterize length that scales linearly with N. This difference in size-scaling creates a packing frustration, thus requires an additional parameter to describe the size mismatch between the rods and coils. In addition, the interplay between the liquid-crystalline ordering of the rod blocks and the microphase separation of the rods and coils

leads to rich and complex phase behavior. Furthermore, the smectic structures can be classified into smectic-A and smectic-C according to the tilt angle θ between the nematic direction and lamellar normal, as well as monolayer, bilayer and folded structures, according to the geometric arrangement of rods. These various smectic microstructures can be greatly affected by the size asymmetry between the rods and coils, as well as the coupling between the isotropic and anisotropic interactions.

Technological applications of rod-coil block copolymers strongly depend on their self-assembled nanostructure and phase behavior. Theoretical studies on these polymers provide convenient means to understand the phase behavior.[17] In what follows we mainly focus on the study of block copolymers using the self-consistent field theory (SCFT), which is a powerful tool for understanding the equilibrium thermodynamics of polymeric systems. Within the SCFT framework, the statistical mechanics of many polymers is transformed into a field theory. The essence of the SCFT includes two ingredients: the statistics of chain conformation described by a propagator $q(\mathbf{r},s)$, and the interactions between molecules modeled by a mean-field potential. In contrast to the simple Gaussian chain model, the wormlike chain model is more general for describing the conformation of polymer chains with a degree of rigidity.[18] Within the wormlike-chain like model, the state of a segment is specified by its position $\mathbf{r}$ and orientation $\mathbf{u}$. In this case, the chain propagator $q(\mathbf{r},\mathbf{u},s)$ satisfies a diffusion-like equation in the six-dimensional (6D) space composed of three-dimensional (3D) position space, two additional internal coordinates describing the segment orientation, and the chain arc length s. Due to the extra internal coordinates, the numerical solution of the 6D diffusion equation presents considerable computational challenges. Additionally, semi-flexible or rigid units in polymer chains can form liquid crystalline nematic and smectic phases, thus possessing spontaneous orientational order commonly described by a nematic director $\mathbf{n}$. Typically, the anisotropic orientational interactions are

[a]Key Laboratory of Molecular Engineering of Polymer, Ministry of Education, Department of Macromolecular Science, Fudan University, Shanghai, 200433, China. E-mail: pingtang@fudan.edu.cn
[b]Department of Physics and Astronomy, McMaster University, Hamilton, L8S 4M1, Canada

described by the Onsager's excluded volume theory[19] or the Maier–Saupe theory.[20–22] Although solving the SCFT equations for block copolymers containing semiflexible blocks is a challenging task, a number of numerical implementations of the SCFT based on a wormlike chain model have been presented in the literature.[17,18,23–25]

One numerical approach to solving the SCFT equations for semiflexible chains is based on the spectral method, in which orientation-dependent functions are expanded in terms of the spherical harmonics $Y_{l,m}(\mathbf{u})$, as used by a number of groups.[18,24–27] This numerical method can be effective for simple cases, but the computation in this approach can be exceedingly costly when a full expansion in terms of $Y_{l,m}(\mathbf{u})$ is required. For simplicity, the previous studies assumed $m = 0$, thus restricting their results to phases with axial-symmetries such as nematic and smectic-A. A complementary numerical implementation based on a real-space method is presented in our previous work.[17] The real-space method utilizes the fact that orientation variable is a unit vector $\mathbf{u}$ located on a unit sphere in a 3D Euclidean space, which can be discretized into a set of nearly uniform triangular lattice points generated by the spherical projection of the regular icosahedron. The diffusion-like equation for $q(\mathbf{r},\mathbf{u},s)$ is solved in real-space by performing a forward time centered space scheme for s and $\mathbf{r}$, and the finite volume algorithm for $\nabla_u^2 q(\mathbf{r},\mathbf{u},s)$ on the unit spherical surface. This approach is a true 3D Euclidean space consideration of the orientation variable, thus the smectic-C phase can be obtained easily. On the other hand, a finite difference method is applied for both $\mathbf{r}$ and s in our previous study,[17] in which the solution accuracy and stability are limited.

In the current paper, as a methodological improvement of our previous work,[17] we report a hybrid numerical approach to the SCFT of semiflexible-coil diblock copolymers. In this method, the spatial dependence of the SCFT functions is expanded in terms of a series of basis functions, instead of finite difference method in real space, to improve the numerical accuracy and stability. Furthermore the energetics of the system includes the orientational interaction between the rods characterized by Maier–Saupe theory instead of Onsager type in our previous paper,[17] and the enthalpic interaction between rods and coils modeled by Flory–Huggins interactions. This treatment of the orientational interactions is generally adopted in rod-coil melts,[26–28] which is more relevant to experimental conditions. Furthermore, this model can be used to describe the coupling of isotropic microphase separation and anisotropic orientation ordering. In the current model, the self-assembly and liquid-crystalline ordering of rod-coil copolymers are governed by four parameters: the Flory–Huggins interaction χN, the Maier–Saupe interaction μN, the coil volume fraction f, and the size asymmetry ratio between rods and coils β. In what follows we focus on the effect of interplay between microphase separation and orientational interaction characterized by the ratio μ/χ, as well as size asymmetry ratio β, on the phase behavior and various microstructures of the smectic phases.

Theoretical model and numerical algorithm

We consider an incompressible melt composed of n monodisperse AB semiflexible-coil diblock copolymer chains confined in a volume V. Each coil A-block has N_c segments with

a statistical segment length a, and each wormlike B-block has N_R segments characterized by a statistical length b and a diameter d. For simplicity, the A and B segments are assumed to have equal monomeric volume, $a^3 = bd^2 = 1/\rho_0$, thus the volume fraction of the coil-blocks is $f = \dfrac{N_C}{N_C + N_R} = \dfrac{N_C}{N}$ and the volume fraction of the wormlike blocks is $1 - f$. The conformation of the αth chain is represented by a space curve $\mathbf{r}_\alpha(s)$ (s is the contour length of the chain scaled by N), where $s = 0 \sim f$ corresponding to the A-blocks modeled as a Gaussian chain, and $s = f \sim 1$ corresponding to the B-blocks modeled as a wormlike chain. A unit vector, $\mathbf{u}_\alpha(s) = \dfrac{1}{Nb} \dfrac{d}{ds} \mathbf{r}_\alpha(s)$, is used to denote the orientation of the αth chain at contour position s, which ensures that each segment has a fixed contour length b. Furthermore, the geometrical size asymmetry between the wormlike and coil blocks is characterized by a parameter $\beta = bN/a(N/6)^{1/2}$.

For the flexible A-blocks, the chain propagator, $q_A(\mathbf{r},s)$, satisfies a modified diffusion equation,

$$\frac{\partial}{\partial s} q_A(\mathbf{r}, s) = \nabla^2 q_A(\mathbf{r}, s) - w_A(\mathbf{r})q_A(\mathbf{r}, s), (0 \leq s \leq f) \quad (1)$$

with the initial condition $q_A(\mathbf{r},0) = 1$. Here $w_A(\mathbf{r})$ is a self-consistent field representing the average interactions exerted to the A-species. On the other hand, the chain propagator of the semiflexible B-blocks, $q_B(\mathbf{r},\mathbf{u},s)$, satisfies a diffusion-like equation:[25]

$$\frac{\partial q_B(\mathbf{r}, \mathbf{u}, s)}{\partial s} = -\beta \mathbf{u} \cdot \nabla_r q_B(\mathbf{r}, \mathbf{u}, s)$$
$$- \left[w_B(\mathbf{r}) - \mathbf{M}(\mathbf{r}) : \left(\mathbf{u}\mathbf{u} - \frac{\mathbf{I}}{3} \right) \right] q_B(\mathbf{r}, \mathbf{u}, s) + \frac{1}{2\kappa} \nabla_u^2 q_B(\mathbf{r}, \mathbf{u}, s),$$
$$(f \leq s \leq 1) \quad (2)$$

with the initial condition $q_B(\mathbf{r},\mathbf{u},f) = q_A(\mathbf{r},f)$. The propagator $q_B(\mathbf{r},\mathbf{u},s)$ corresponds to the probability of finding the sth B-block at position $\mathbf{r}$ and with an orientation $\mathbf{u}$ in an external potential field $w_B(\mathbf{r})$ and an orientational field $\mathbf{M}(\mathbf{r})$. The parameter κ represents the bending rigidity, which is nondimensionalized by N and set as $\kappa = 30$ to model a rigid B-block, consistent with our previous study.[17] Because the two ends of the diblock copolymer are distinct, a set of conjugate propagators, $q_A^+(\mathbf{r},s)$ ($0 \leq s \leq f$) and $q_B^+(\mathbf{r},\mathbf{u},s)$ ($f \leq s \leq 1$), are required to complete the description of the chain conformations. These conjugate propagators satisfy the same diffusion equations, eqn (1) and (2), but with different initial conditions, $q_B^+(\mathbf{r},\mathbf{u},1) = 1$ and $q_A^+(\mathbf{r},f) = \dfrac{1}{4\pi} \int d\mathbf{u} q_B^+(\mathbf{r}, \mathbf{u}, f)$. Finally the partition function of a single diblock copolymer chain can be obtained as $Q = \dfrac{1}{4\pi V} \int d\mathbf{r} \int d\mathbf{u} q_B(\mathbf{r}, \mathbf{u}, 1)$. In the above expressions, all spatial lengths are scaled by the unperturbed radius of gyration of the diblock copolymer chains, $R_g = a(N/6)^{1/2}$. Within the SCFT framework, the Helmholtz free energy of the system is given by:

$$\frac{F}{nk_BT} = -\ln Q + \frac{1}{V} \int d\mathbf{r}[\chi N\phi_A\phi_B - w_A\phi_A - w_B\phi_B$$
$$+ \frac{1}{2}\mathbf{M} : \mathbf{S} - \xi(1 - \phi_A - \phi_B)] \quad (3)$$

where $\phi_A(\mathbf{r})$ and $\phi_B(\mathbf{r})$ are density fields normalized by the local volume fractions of the A- and B-blocks, and χ is the Flory–Huggins interaction parameter describing the A–B interactions.

The orientational order-parameter tensor $\mathbf{S}(\mathbf{r})$ and the corresponding self-consistent field $\mathbf{M}(\mathbf{r})$ are spatial-dependent, symmetric and traceless, 3×3 matrices. Finally the function $\xi(\mathbf{r})$ is a potential field that ensures the incompressibility of the system. Minimizing the free energy in eqn (3) with respect to ϕ_A, ϕ_B, w_A, w_B, $\mathbf{S}$, $\mathbf{M}$ and ξ leads to the following SCFT equations that describe the equilibrium morphology,

$$w_A(\mathbf{r}) = \chi N \phi_B(\mathbf{r}) + \xi(\mathbf{r}) \tag{4}$$

$$w_B(\mathbf{r}) = \chi N \phi_A(\mathbf{r}) + \xi(\mathbf{r}) \tag{5}$$

$$\phi_A(\mathbf{r}) = \frac{1}{Q}\int_0^f ds\, q_A(\mathbf{r},s)q_A^+(\mathbf{r},s) \tag{6}$$

$$\phi_B(\mathbf{r}) = \frac{1}{4\pi Q}\int_f^1 ds \int d\mathbf{u}\, q_B(\mathbf{r},\mathbf{u},s)q_B^+(\mathbf{r},\mathbf{u},s) \tag{7}$$

$$\mathbf{S}(\mathbf{r}) = \frac{1}{4\pi Q}\int_f^1 ds \int d\mathbf{u}\, q_B(\mathbf{r},\mathbf{u},s)q_B^+(\mathbf{r},\mathbf{u},s)\left(\mathbf{uu} - \frac{\mathbf{I}}{3}\right) \tag{8}$$

$$\mathbf{M}(\mathbf{r}) = \mu N \mathbf{S}(\mathbf{r}) \tag{9}$$

$$\phi_A(\mathbf{r}) + \phi_B(\mathbf{r}) = 1 \tag{10}$$

The anisotropic interactions between the wormlike blocks are quantified by the Maier–Saupe mean-field potential in eqn (9), where μ characterizes the strength of the orientational interaction favoring the alignment of the segments. The most time-consuming step in solving the SCFT equations, eqn (1)–(10), is to compute the propagators by solving the diffusion-like equations, eqn (1) and (2). For the Gaussian chain propagator defined in eqn (1), several efficient numerical methods have been developed.[29–31] However solution of the diffusion equation of wormlike chains is quite difficult to obtain. In what follows a hybrid numerical implementation SCFT for wormlike chain model will be used. Similar to our previous work,[17] the Laplacian on the unit spherical surface, $\nabla_\mathbf{u}^2 q_B(\mathbf{r},\mathbf{u},s)$, is implemented using the finite volume algorithm. On the other hand, all spatial-dependent functions are expanded in terms of suitable basis functions,

$$g(\mathbf{r}) = \sum_i g_i f_i(\mathbf{r}) \tag{11}$$

where the basis functions, $f_i(\mathbf{r})$ for $i = 1,2,3\ldots$, are chosen such that they are orthonormal and eigenfunctions of the Laplacian operators.

$$\frac{1}{V}\int d\mathbf{r} f_i(\mathbf{r})f_j(\mathbf{r}) = \delta_{ij}, \quad \nabla_\mathbf{r}^2 f_i(\mathbf{r}) = -\lambda_i f_i(\mathbf{r}) \tag{12}$$

As a first step of applying the hybrid method, in the current paper we focus on the liquid-crystalline behavior of lamellar phases self-assembled from semiflexible-coil diblock copolymer melts. Therefore all spatial-dependent functions are functions of z only, and the basis functions for this case can be chosen as follows:

$$f_i(z) = 1, \sqrt{2}\cos\left(\frac{2\pi z}{D}\right), \sqrt{2}\sin\left(\frac{2\pi z}{D}\right), \sqrt{2}\cos\left(\frac{4\pi z}{D}\right),$$
$$\sqrt{2}\sin\left(\frac{4\pi z}{D}\right)\cdots \tag{13}$$

where D is the period of the ordered phases and z is the spatial coordinate. The z-dependent functions can be expanded by $f_i(z)$ as,

$$q_A(z,s) = \sum_i q_{A,i}(s)f_i(z), \quad q_A^+(z,s) = \sum_i q_{A,i}^+(s)f_i(z) \tag{14}$$

$$q_B(z,\mathbf{u},s) = \sum_i q_{B,i}(\mathbf{u},s)f_i(z), \quad q_B^+(z,\mathbf{u},s) = \sum_i q_{B,i}^+(\mathbf{u},s)f_i(z) \tag{15}$$

$$\phi_A(z) = \sum_i \phi_{A,i} f_i(z), \quad \phi_B(z) = \sum_i \phi_{B,i} f_i(z) \tag{16}$$

$$w_A(z) = \sum_i w_{A,i} f_i(z), \quad w_B(z) = \sum_i w_{B,i} f_i(z) \tag{17}$$

$$\mathbf{S}(z) = \sum_i \mathbf{S}_i f_i(z), \quad \mathbf{M}(z) = \sum_i \mathbf{M}_i f_i(z) \tag{18}$$

$$\xi(z) = \sum_i \xi_i f_i(z) \tag{19}$$

The differential equations for the end-segment distribution functions become,

$$\frac{\partial q_{A,i}(s)}{\partial s} = -\lambda_i q_{A,i}(s) - \sum_j \sum_k \Gamma_{ijk} q_{A,j}(s)w_{A,k} \tag{20}$$
$$q_{A,i}(0) = \delta_{i1}$$

$$\frac{\partial q_{B,i}(\mathbf{u},s)}{\partial s} = -\beta\mathbf{u}\sum_j A_{ij}q_{B,j}(\mathbf{u},s) + \frac{1}{2\kappa}\nabla_\mathbf{u}^2 q_{B,i}(\mathbf{u},s)$$
$$- \sum_j \sum_k \Gamma_{ijk}\left[w_{B,k} - \mathbf{M}_k : \left(\mathbf{uu} - \frac{\mathbf{I}}{3}\right)\right]q_{B,j}(\mathbf{u},s)$$
$$q_{B,i}(\mathbf{u},f) = q_{A,i}(f) \tag{21}$$

$$\frac{\partial q_{B,i}^+(\mathbf{u},s)}{\partial s} = -\beta\mathbf{u}\sum_j A_{ij}q_{B,j}^+(\mathbf{u},s) - \frac{1}{2\kappa}\nabla_\mathbf{u}^2 q_{B,i}^+(\mathbf{u},s)$$
$$+ \sum_j \sum_k \Gamma_{ijk}\left[w_{B,k} - \mathbf{M}_k : \left(\mathbf{uu} - \frac{\mathbf{I}}{3}\right)\right]q_{B,j}^+(\mathbf{u},s)$$
$$q_{B,i}^+(\mathbf{u},1) = \delta_{i1} \tag{22}$$

$$\frac{\partial q_{A,i}^+(s)}{\partial s} = \lambda_i q_{A,i}^+(s) + \sum_j \sum_k \Gamma_{ijk}q_{A,j}^+(s)w_{A,k}$$
$$q_{A,i}^+(f) = \frac{1}{4\pi}\int d\mathbf{u}\, q_{B,i}^+(\mathbf{u},f) \tag{23}$$

with

$$\lambda_i = \begin{cases} 0 & \text{if } i = 1 \\ \left(\dfrac{i\pi}{D}\right)^2 & \text{if } i \text{ even} \\ \left(\dfrac{(i-1)\pi}{D}\right)^2 & \text{if } i \text{ odd} \end{cases} \qquad (24)$$

$$A_{ij} = \frac{1}{D}\int dz f_i(z)\nabla f_j(z) \qquad (25)$$

$$\Gamma_{ijk} = \frac{1}{D}\int dz f_i(z)f_j(z)f_k(z) \qquad (26)$$

where Γ_{ijk} is a symmetric tensor, and A_{ij} is an antisymmetric matrix. The partition function of a single diblock copolymer chain in the potential fields $w_A(z)$, $w_B(z)$, $\mathbf{M}(z)$ and $\xi(z)$ is given by $Q = \frac{1}{4\pi}\int d\mathbf{u} q_{B,1}(\mathbf{u}, 1)$. The amplitudes of $\phi_A(z)$, $\phi_B(z)$, $w_A(z)$, $w_B(z)$, $\mathbf{S}(z)$ and $\mathbf{M}(z)$ are given by:

$$\phi_{A,i} = \frac{1}{Q}\int_0^f ds \sum_j \sum_k q_{A,j}(s)q_{A,k}^+(s)\Gamma_{ijk} \qquad (27)$$

$$\phi_{B,i} = \frac{1}{4\pi Q}\int_f^1 ds \int d\mathbf{u} \sum_j \sum_k q_{B,j}(\mathbf{u},s)q_{B,k}^+(\mathbf{u},s)\Gamma_{ijk} \qquad (28)$$

$$w_{A,i} = \chi N(\phi_{B,i} - \delta_{i1}(1-f)) + \xi_i \qquad (29)$$

$$w_{B,i} = \chi N(\phi_{A,i} - \delta_{i1}f) + \xi_i \qquad (30)$$

$$\mathbf{S}_i = \frac{1}{4\pi Q}\int_f^1 ds \int d\mathbf{u} \sum_j \sum_k q_{B,j}(\mathbf{u},s)q_{B,k}^+(\mathbf{u},s)\left(\mathbf{uu} - \frac{\mathbf{I}}{3}\right)\Gamma_{ijk} \qquad (31)$$

$$\mathbf{M}_i = \mu N \mathbf{S}_i \qquad (32)$$

$$\phi_{A,i} + \phi_{B,i} = \delta_{i1} \qquad (33)$$

where ξ_i in eqn (19) is chosen to be $\xi_i = \lambda(\phi_{A,i} + \phi_{B,i} - \delta_{i1})$, where λ is large enough to enforce the incompressibility of the system. Finally, the free energy function of the system can be expressed in terms of the expansion coefficients:

$$\frac{F}{nk_BT} = -\ln Q + \sum_i \left(\chi N \phi_{A,i}\phi_{B,i} - w_{A,i}\phi_{A,i} - w_{B,i}\phi_{B,i} + \frac{1}{2}\mathbf{M}_i : \mathbf{S}_i \right) \qquad (34)$$

The set of SCFT equations is reduced to those composed of the expansion coefficients. The potential and orientational fields are updated using eqn (29), (30) and (32) by means of a linear mixing of new and old solutions. These steps are repeated until self-consistency is achieved. In each step, the key procedure is the solution of propagator coefficients in diffusion-like equations (20)–(23). Both $\nabla_u^2 q_{B,i}(\mathbf{u},s)$ and $\nabla_u^2 q_{B,i}^+(\mathbf{u},s)$ are calculated by the finite volume algorithm using the orientation variable $\mathbf{u}$ discretized on the surface of a unit sphere triangulated with $N_u = 92$

vertexes. The number of basis functions is changed over $N_i = 13$–25 under different interactions, to ensure that the free energy is converged in the order of 10^{-4}. Additionally we use $N_s = 800$ contour points resolving the s dependence, to ensure the discretization of $\Delta s = 1/N_s$ sufficient to obtain accuracy of the order of 10^{-6} in the potential fields (including compositional and orientational potentials). In this case, it requires an operation count of $O(N_s N_u N_i^3)$ and time consumption of $6\sim30s$ per Δs step. The solution for each iteration in a certain period length D and tilt angle θ is proven to rapidly achieve self-consistence within 2000 steps. Finally the equilibrium morphology is obtained according to the minimization of free energy iterated with respect to variety of reasonable sizes of the simulation cell and different initial guess of the orientational direction.

We should note that, the extension to 2D and 3D space is straightforward by the hybrid numerical approach, without any complexity in algorithm required to solve SCFT equations. The basis functions used to expand the spatial dependence generally take on a form as $f_j(\mathbf{r}) = \exp(i\mathbf{G}_j\cdot\mathbf{r})$. In the 3D case, the wave vector $\mathbf{G}_j$ is defined by $\mathbf{G}_j = 2\pi\left(\dfrac{h_j}{D_x}, \dfrac{k_j}{D_y}, \dfrac{l_j}{D_z}\right)$, where D_x, D_y, D_z are the sizes of the rectangular box in 3D real space, and integers $h_j, k_j, l_j = 0, \pm1, \pm2\ldots$ For simplicity in the 1D case, $h = k = 0$, $l = 0, 1, 2\ldots$ and we split $\exp(i\mathbf{G}_j\cdot\mathbf{r})$ into $g_j\sin(\mathbf{G}_j\cdot\mathbf{r})$ and $g_j\cos(\mathbf{G}_j\cdot\mathbf{r})$ as in eqn (13). For the case of 3D space, just with the details of $\mathbf{G}_j$, $f_j(\mathbf{r})$ and A_{ij}, Γ_{ijk} being changed correspondingly. Furthermore, the algorithm is similar to that of 1D case when introducing h and k to $\mathbf{G}$, and the computational time is still determined by the number of basis functions N_i, which depends on the symmetry and complexity of ordered microstructures. Our preliminary tests prove this method to converge more rapidly than finite different techniques for spatial discretization in our previous paper[17] and have high accuracy with a suitable truncation of basis functions N_i. Further work on this will be done.

Results and discussion

In the following studies the nematic ordering is assumed to be uniaxial, thus the liquid-crystalline order is described by the nematic director $\mathbf{n}$, which is along the z-axis for the smectic-A ($\theta = 0$) phase or tilted with an angle from the z-axis for the smectic-C ($\theta \neq 0$) phase. The orientational order can be quantified by the zz component of the orientational tensor $\mathbf{S}(z)$, i.e., $S_{zz}(z)$. When normalized by the volume fraction of the wormlike blocks $\phi_B(z)$, $S_{zz}(z)$ varies from 0 (representing random orientation of the wormlike blocks) to 1 (representing complete alignment of the wormlike blocks). Deviation of $S_{zz}(z)$ from unity characterized the degree of disalignment of the wormlike blocks. A distinct transition from the isotropic phase ($S_{zz}(z) = 0$) to the nematic phases ($S_{zz}(z) \neq 0$) can be distinguished from the behavior of the orientation order parameter. Furthermore, monolayer, bilayer and folded smectic phases of the wormlike blocks are obtained, indicating different packing geometry of the semiflexible blocks. We should note that these complex 1D ordered phases were not found in our previous study of rod-coil using Onsager excluded volume interaction,[17] and hence their dependence on parameters including χN, μN, f and β will be systematically discussed in the following subsections.

A. Interplay between A-B repulsion and liquid-crystalline ordering: the case of $\mu/\chi = 4$

The phases and phase transitions of semiflexible-coil diblock copolymers depend strongly on the repulsion between the wormlike and coil blocks characterized by the Flory–Huggins parameter χ and the orienting interaction characterized by the Maier–Saupe parameter μ. In this subsection the case of strong orienting interaction is considered by examining the phase diagram $\mu/\chi = 4$ with varying χN and f. This particular ratio of $\mu/\chi = 4$ was used in a previous study by Pryamitsyn and Ganesan for rod-coil diblock copolymers,[28] so a direct comparison with this previous work can be made. Phase diagrams of the semiflexible-coil diblock copolymers with three different values of $\beta = 2$, $\beta = 4$ and $\beta = 10$ are constructed, as presented in Fig. 1.

Isotropic and nematic phases. The isotropic region in the phase diagram shown in Fig. 1 remains almost unchanged for the different values of β. The nematic region is quite narrow and shrinking with the increase of β. This behavior is in agreement with the prediction of Pryamitsyn and Ganesan[28] for the case of rigid rod-coil diblock copolymers. On the other hand, rod-coil block copolymers can exhibit a wider nematic region under relatively strong orientational interactions, as has been seen both in experiments[15] and Onsager theoretical model.[17,26] The narrow nematic region shown in Fig. 1 indicates that the ratio of $\mu/\chi = 4$

may be much smaller than that corresponding to the experimental systems (with a wider nematic region) in the weak segregation limit. This point will be further investigated in the following discussions.[15]

Order–disorder transitions. As the temperature is lowered (or the χN and μN are increased), order–disorder transitions (ODT), corresponding to phase transitions from the spatially disordered (isotropic or nematic) phases to spatially ordered (smectic) phases, can be induced. Within the mean-field theory, the nematic–smectic transition is generally continuous and the isotropic–smectic transition is a first-order one. The phase diagrams shown in Fig. 1 reveal that the ODT is relatively insensitive to β, with a small difference in the nematic–smectic transition at relatively low volume fractions of the coils. It is interesting to notice that as β decreases from $\beta = 10$ to $\beta = 2$, the nematic region expands slightly, resulting in a higher χN_{ODT} for the nematic–smectic phase transition. This observation is in accordance with the prediction by Matsen and Barrett[27] about the dependence of χN_{ODT} on the size asymmetry parameter $v = \sqrt{6}\beta^{-1}$, in which the nematic–smectic transition is relatively insensitive to v until $v \approx 1$ ($\beta = 2.45$).

Order–order transition. In the current study only 1D ordered phases are considered. Therefore, the order–order transitions (OOT) include smectic-A to smectic-C with various
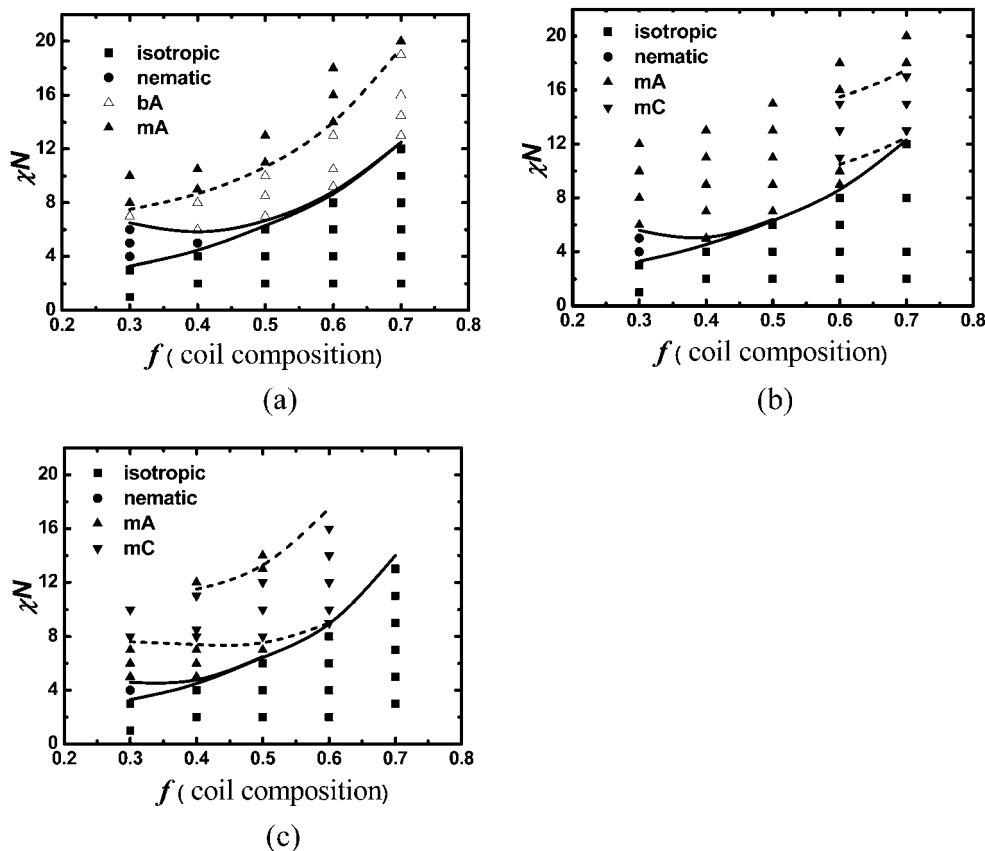

Fig. 1 Phase diagrams of rod-coil block copolymers at $\mu/\chi = 4$. (a) $\beta = 2$; (b) $\beta = 4$; (c) $\beta = 10$. Solid lines are a guide to the eye denoting phase boundaries of isotropic–nematic, isotropic–smectic, and nematic–smectic transitions. Dashed lines are used to separate bilayer smectic-A (bA) from monolayer smectic-A (mA) in (a), monolayer smectic-C (mC) from monolayer smectic-A (mA) in (b) and (c).

microstructures of rod molecules. As shown in the phase diagrams (Fig. 1), a number of ordered microstructures of the smectic phases, including monolayer smectic-A (mA), monolayer smectic-C (mC) and bilayer smectic-A (bA), have been observed for the parameters examined in this section. For the monolayer smectic phases, the head and tail of the rod-like molecules are randomly distributed, interdigitating within the layer containing the wormlike blocks. This phase was referred as the partial bilayer structures by Duch and Sullivan.[24] For the bilayer structures, the rod-like blocks are arranged antiparallelly, *i.e.* end-to-end in the rod-layers. Various architectures for the smectic phases can be clearly distinguished by the spatial distribution of the individual rod segments $\varphi(z,s)$, which is defined by,

$$\varphi(z,s) = \frac{1}{4\pi Q} \int d\mathbf{u} q_{\mathrm{B}}(z,\mathbf{u},s) q_{\mathrm{B}}^{+}(z,\mathbf{u},s) \ (f \leq s \leq 1) \quad (35)$$

Monolayer smectic phases. For the case of $\beta = 4$ and $\beta = 10$, the monolayer structures can be classified into monolayer smectic-A (mA) with $\theta = 0$ and monolayer smectic-C (mC) with $\theta \neq 0$. The occurrence of the mA and mC phases in the phase space of χN (μN) *vs. f* depends on the competition between the microphase separation and the orientational interaction. In order to provide insight into the architectures of monolayer smectic phase, a moderate value of $\beta = 4$ in Fig. 1(b) is used as an example to illustrate the structure and phase behavior of the system.

Fig. 2(a) presents the profiles of mA at $\chi N = 10$ ($\mu/\chi = 4$) with $f = 0.4$. The density of the rod-like blocks reaches its saturation value in the rod-rich area, thus the coil segments are expelled from this region completely. At the same time, the orientation order parameter $S_{zz}(z)$ approaches unity within the rod-rich area, indicating a strong degree of orientation order. Information about the packing of the rod-like blocks is revealed from the spatial distribution of the end segment of the rods, $\varphi(z,s = 1)$, which is shown in Fig. 2. For the current case, two peaks are found at the lamellar interface and the average distance between these two peaks is slightly smaller than the contour length of the rod-like blocks, indicating an almost complete interdigitation between the rods and the formation of monolayer smectic-A structure. This observation is in agreement with the prediction of partial bilayer by Duch and Sullivan[24] using the Onsager excluded-volume interaction. Furthermore, the lamellar period

of mA at $f = 0.4$ decreases from $D = 4.8R_g$ at $\chi N_{\mathrm{ODT}} = 5$ to $D = 3.4R_g$ at $\chi N = 10$, indicating a better ordering of the rod-like blocks at higher Maier–Saupe interaction and stronger separation between the rods and coils. It is also noticed that the scaling behavior is in agreement with the prediction by Matsen and Barrett ($D/bN^{1/2} \sim v^{-1}$, *viz.*, $D/R_g \sim \beta$).[27]

For the case of coil composition $f = 0.6$, the stretching energy of the coil blocks becomes a dominant factor, which favors a large interfacial area per chain. As a result, a smectic-C phase with a non-zero tilt angle $\theta \neq 0$ appears in order to increase the interfacial area, as shown in Fig. 2(b). These structural changes are illustrated in the example shown in Fig. 2(b), in which the smectic-C phase has a lamellar period of $D = 3.2R_g$ and a tilt angle of $\theta = 30°$ at $\chi N = 14$. The structure of the mC phase is characterized by the spatial density distribution of the end segment of rods, $\varphi(z,s = 1)$, shown in Fig. 2(b). The lamellae period is related to the tilt angle θ, *i.e.*, $D/Rg \sim \beta \cos\theta$, indicating that the period of the monolayer smectic phases (mA and mC) is largely determined by the parameter β. Furthermore, it is noticed that the tilt angle tends to decrease as χN (μN) is increased, until it vanishes ($\theta = 0$), leading to a re-entrance mC–mA transition as shown in Fig. 1(b). This re-entrance transition has been considered in previous theory.[32] The observation of the series of transitions from isotropic to smectic-A and then to smectic-C and finally to smectic-A has also been predicted by Matsen and Barrett[27] in rod-coil copolymers with $v = 0.5$, corresponding to $\beta \simeq 5$ in the current model.

Bilayer smectic-A phases (bA). For the case of $\beta = 2$, two smectic-A phases (mA and bA) are observed as the ordered structures, as shown in Fig. 1(a). The bA phase generally occurs near the ODT, or the nematic–smectic and isotropic–smectic transition lines, where the rods and coils are partially miscible forming diffuse interfaces. With the increasing of $\mu N(\chi N)$, the bA phase can continuously transform to the mA phase when the rod-like blocks packing changes continuously from end-to-end arrangement to complete interdigitation. For simplicity the partial interdigitation configuration is referred as monolayer structure in the current paper.

Fig. 3 provides a comparison of the bA profiles at two different volume fractions, $f = 0.4$ and $f = 0.6$. First of all, the distribution of the rod-end segments, $\varphi(z,s = 1)$, exhibits one peak in the middle of the rod-rich domain, clearly showing an end-to-end arrangement of the rod-like blocks. Secondly the distribution of
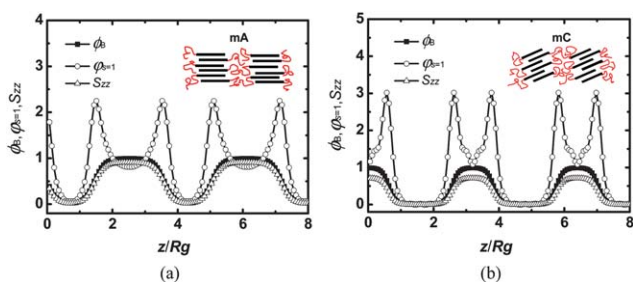

Fig. 2 Plots of $\phi_B(z)$, $\varphi(z,s = 1)$ (rod terminal) and $S_{zz}(z)$ for monolayer smectic phase under $\beta = 4$ and $\mu/\chi = 4$. (a) monolayer smectic-A (mA) with $f = 0.4$, $\chi N = 10$ and $D = 3.6R_g$; (b) monolayer smectic-C (mC) with $f = 0.6$, $\chi N = 14$, $D = 3.2R_g$ and $\theta = 30°$.
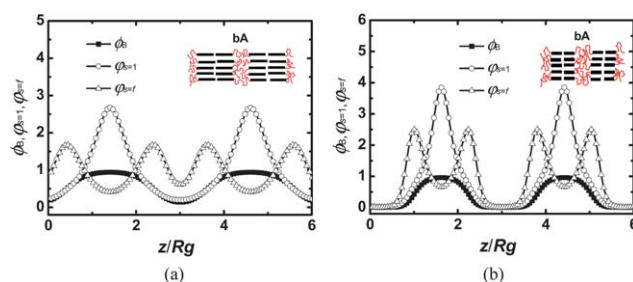

Fig. 3 Plots of $\phi_B(z)$, $\varphi(z,s = 1)$ (rod terminal) and $\varphi(z,s = f)$ for bilayer smectic-A phases (bA) under $\beta = 2$ and $\mu/\chi = 4$. (a) $f = 0.4$, $\chi N = 7$ and $D = 3.2R_g$; (b) $f = 0.6$, $\chi N = 12$ and $D = 2.8R_g$.

the rod-coil linking segments, $\varphi(z,s = f)$, has two peaks approximately located at the rod-coil interfaces. The distance between these two peaks is slightly smaller than twice the rod length, suggesting some degree of disalignment of the rods in the bA structure, which increases the interfacial area per chain favoring coil-stretching energy than the case of well-aligned rods under large μN. The observation of the bilayer smectic phases for $\beta = 2$ suggests that the rod-like molecules with larger diameter tend to form end-to-end arrangement, in contrast to the thinner ones such as $\beta = 4$ and $\beta = 10$. This size asymmetry effect can be understood from the competition between interfacial energy and coil-stretching entropy.

However there exist some discrepancies in the bA and mA regions between Fig. 1(a) and previous SCFT studies,[27,28] which may be attributed to the differences in chain models for the rod-like blocks and different orientational interaction treatments. Semenov[33] and Matsen and Barrett,[27] as well as Pryamitsyn and Ganesan[28] assumed completely rigid rods, thus ignoring the conformational entropy of the rod-like blocks. Based on the Semenov–Vasilenko model and SCFT, Matsen and Barrett assumed a "hard" Flory interaction between the rods and observed the bA phase at extremely large χN and small f. Pryamitsyn and Ganesan observed some metastable bilayers at relatively small χN and f with a system of large β. In contrast, the model system in current study considers wormlike chain conformation with large rod diameter ($\beta = 2$) and assumes $\mu/\chi = 4$, where the orientational interaction is more significant than microphase separation. Therefore in the weak-segregation regime (small χN and hence small μN), the rod-like blocks exhibit some degree of chain bending fluctuation and disalignment along the nematic director leading to interfacial area per chain. This can be approved by the zz component of the order parameter tensor $S(z)$ (figures of $S_{zz}(z)$ are not shown here), where the overall orientational degree in the bilayer decreases from the rod-rich area to the rod-coil interface, different from the case of completely rigid rods. In this case, therefore enough large interfacial area per chain favors the coil-stretching entropy and stabilizes the bA structure even at relatively high coil volume fraction such as $f = 0.6$, as shown in Fig. 3(b). However with the increasing of μN, the rods are well oriented leading to an obvious decrease of surface area per chain in bA. As a result, the rods tend to interdigitate with each other in order to increase the surface area for coil-stretching entropy, leading to a transformation from bA to mA. The bA to mA transition in this case is driven by the Maier–Saupe interactions between rods and relatively small β, while χN effect can be ignored.

B. Comparable A–B repulsion and orientational interactions ($\mu/\chi = 1$)

In this subsection the case with compatible rod-coil repulsion and orientational interaction ($\mu/\chi = 1$) is considered. Phase diagrams with $\mu/\chi = 1$ for $\beta = 4$ and $\beta = 10$ are shown in Fig. 4. In contrast to the phase diagrams with $\mu/\chi = 4$ (Fig. 1), the weaker orientational interaction leads to the formation of a lamellar phase without a liquid-crystalline order. This lamellar phase is similar to the lamellae found in the coil-coil dilbock copolymers. When μN is increased, the rod-like blocks can acquire a nematic order as shown in the last subsection. This
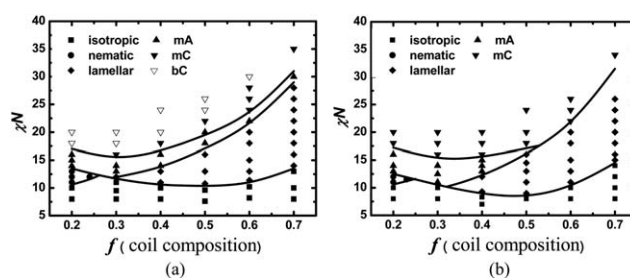

Fig. 4 Phase diagrams of rod-coil block copolymers with $\mu/\chi = 1$. (a) $\beta = 4$; (b) $\beta = 10$. Solid lines are a guide to the eye denoting phase boundaries. Different triangles represent various smectic phases such as monolayer smectic-A (mA), monolayer smectic-C (mC) and bilayer smectic-C (bC).

behavior is consistent with the predictions by Landau expansions[26] and experimental observations.[16] The lamellar region is larger in Fig. 4(b) compared to that in Fig. 4(a), due to the lower ODT χN_{ODT} for the isotropic–lamellar transition for $\beta = 10$ than that for $\beta = 4$. The lamellar structure disappears with the decreasing of f, leading to a triple point f_{tri} at which the isotropic, lamellar and smectic phases coexist. When the coil composition is less than the triple point, $f < f_{tri}$, a direct transition from the isotropic phase to the smectic phase occurs. With further decrease of f, the isotropic phase directly transforms to the nematic phase due to the strong ordering effects of the rod-like blocks. The narrow nematic region and the size asymmetry effect on the nematic region are similar to the case of $\mu/\chi = 4$. Moreover, the lamellar period is obviously larger than that of the corresponding coil-coil diblock copolymers. For example, in the case of $\beta = 4$, with the increasing of χN and hence μN, the lamellar spacing increases from $3.0R_g$ to $4.4R_g$ for $f = 0.6$ and $2.8R_g$ to $4.0R_g$ for $f = 0.7$, respectively. According to the spatial distribution of the individual B segments $\varphi(z,s)$, we can probe into the architecture of the B blocks in the lamellae. For brevity the calculation results are not shown here, in which we found that the terminal and middle segments of the B blocks exhibit a diffusive distribution in the centre of rod-rich area under small μN (χN), suggesting nearly random configuration of the B block like coils. As the enhancement of orientational interactions, the B-blocks stretch obviously and align along the nematic direction **n**, as shown by the two peaks in the spatial distribution of the end of rods $\varphi(z,s = 1)$ and the increasing of order parameter $\bar{S}_{zz}$. This leads to an expansion of rod domain size, and correspondingly the increasing of the lamellar period.

One interesting new phase from the current SCFT study is a structure composed of bilayer smectic-C (bC), which is found for $\beta = 4$ as shown in the phase diagram (Fig. 4(a)). In this phase the rod-like blocks pack in an end-to-end fashion and tilt away from the z-axis. This phase has not been found in previous SCFT studies with the assumption of completely rigid rods.[27,28] The phase diagram in Fig. 4(a) exhibits three smectic phases including mA, mC and bC. In general, the system can undergo a series of transitions, from mA to mC, and then to bC phase, with the increasing of χN and μN. These phase transitions are driven by the competition between the coil-stretching entropy and interfacial energy. When the coil-stretching entropy dominates, the mC phase is more stable as it can supply larger interfacial area;

while bC phase is preferred when the interfacial energy dominates in strong-segregation regime. This is different from the observation of bA in weak-segregation regime in Fig. 1(a), where the Maier–Saupe orientational interaction is dominant for $\mu/\chi = 4$. Therefore we conclude that the interplay between μN and χN combined with β can largely affect the competition between coil-stretching entropy and interfacial energy, leading to the monolayer and bilayer phases occurring in different region of the phase diagram. Moreover, mC and bC phases disappear at $f = 0.2$ and $f = 0.7$, respectively. The mC phase occupies a large area of the phase diagram for $\beta = 10$ in Fig. 4(b) whereas the bC phase occupies a large area for $\beta = 4$ in Fig. 4(a). This behavior is similar to the case of $\mu/\chi = 4$ shown in Fig. 1.

C. When microphase separation is turned off ($\chi N = 0$)

In this subsection the case $\chi N = 0$ is examined. In this case the repulsion between the rod-like and coil blocks is turned off, thus only the Maier–Saupe orientational interaction and chain rigidity are responsible for the phase behavior. The phase diagrams in the μN vs. f plane for this case are presented in Fig. 5 with $\beta = 4$ in Fig. 5(a) and $\beta = 10$ in Fig. 5(b). Fig. 5 shows that, in the absence of the block repulsion, the system can exhibit various liquid crystal phases including isotropic, nematic and smectic phases. Phase transitions can be induced by the increase of the Maier–Saupe orientational interaction μN. The nematic phase in the phase diagram in Fig. 5 occupies a larger region when compared with Fig. 1 for $\mu/\chi = 4$ and Fig. 4 for $\mu/\chi = 1$. This result is qualitatively in agreement with that of Landau free energy theory[26] and our previous SCFT studies of rod-coil block copolymers with Onsager excluded volume interactions[17] and by Duchs and Sullivan,[24] as well as experimental results[14,15] in weak segregation limit (quite small $|\chi N|$). To our knowledge, the above observation is the first demonstration of typical liquid-crystalline behavior from semiflexible-coil diblock copolymers only with Maier–Saupe orientational interaction μN.

As shown in Fig. 5, the isotropic–nematic and isotropic–smectic transitions (LCT) are not sensitive to the size asymmetry parameter β. On the other hand, the χN_{ODT} for the nematic–smectic transition increases sharply as β decreases from $\beta = 10$ to $\beta = 4$ at small f, leading to an enlarged nematic region in the phase diagram at $\beta = 4$. Furthermore, only smectic-A is observed in Fig. 5(a) for $\beta = 4$ compared to the occurrence of both smectic-
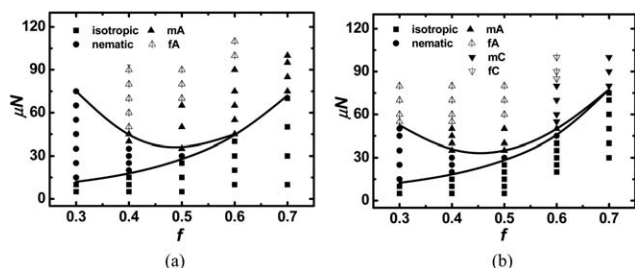
A and smectic-C phases in Fig. 5(b) for $\beta = 10$, which is similar to that in Fig. 1(b) and Fig. 1(c). The phase transition between smectic-A and smectic-C for $\beta = 10$ largely depends on the ratio μ/χ. When the orientational interactions between the rod-like blocks dominate with the absence of rod-coil repulsion, the smectic-A to smectic-C transition is sensitive to the coil composition f, exposing a phase boundary at approximately $f = 0.5$–0.6 as shown in Fig. 5(b); meanwhile when the rod-coil repulsion is non-zero, the smectic-A to smectic-C transition tends to be more sensitive to χN. This difference indicates that not only β but also μ/χ affects the smectic microstructures and order–order transitions of the semiflexible-coil diblock melts.

One interesting phase is the folded smectic microstructure observed at relatively large volume fraction of the rod-like blocks $(1 - f \geq 0.4)$ and strong Maier–Saupe interactions (Fig. 5). Similar structures have been identified in polymeric rod-coil systems from earlier experimental studies,[9,34] but have not been predicted in previous theoretical studies including our own study[17] using the Onsager excluded volume interaction. The folded configuration for the rod-like blocks based on the wormlike chain model resembles the crystalline behavior of semiflexible polymers.[25] Fig. 6 shows typical density profiles of folded smectic-A (fA) phase for $\beta = 10$. The domain size of the rod-rich area can be estimated by computing the spatial distribution of individual rod segments $\varphi(z,s)$. For $f = 0.4$ in Fig. 6(a), the rod-like block folds twice according to the distance between two peaks of $\varphi(z,s = f)$, which is $2.18R_g$ across the rod domain and approximately 1/3 of the rod contour length $6.0R_g$. Meanwhile density distribution of the end segments of the rod-like blocks $\varphi(z,s = 1)$ exhibits a broad distribution and that of the mid segments $\varphi(z,s = (f + 1)/2)$ exhibits one peak in the middle of rod-rich domain. The insets of Fig. 6(a) and 6 (b) show the schematic pictures of fA: the fold number decreases as the rod volume fraction increases, i.e., fold once with $1 - f = 0.5$ in Fig. 6(b) and fold twice with $1 - f = 0.6$ in Fig. 6(a) under the same μN. This result is qualitatively in agreement with the observation in experiments with the increasing of the helix rod length.[9] Further decreasing of volume fraction of rods (such as $1 - f = 0.3$) will lead to the appearance of mC instead of folded smectic phase in Fig. 5(b). Furthermore, the average fold number per rod-like block is found to increase as the orientational interaction becomes stronger (figures not shown here). This behavior can be attributed to the fact that a stronger Maier–Saupe interaction leads to tighter packing of the rod-like blocks. However this will decrease the area per chain thus increase the stretching energy of
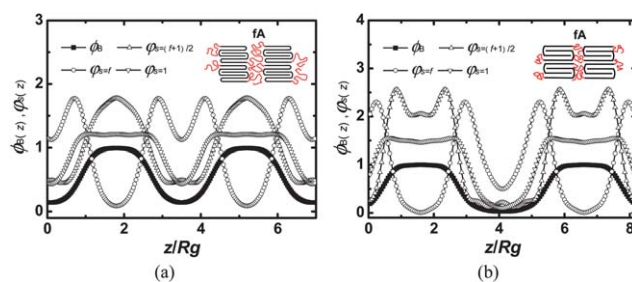

Fig. 5 Phase diagrams of two rod-coil systems as a function of μN and f, with an assumption of $\chi N = 0$. (a) $\beta = 4$; (b) $\beta = 10$. Lines making phase boundaries are a guide to the eye only and different triangles represent various smectic phases such as monolayer smectic-A (mA), monolayer smectic-C (mC), folded smectic-A (fA) and folded smectic-C (fC).

Fig. 6 Plots of $\phi_B(z)$, $\varphi(z,s = f)$, $\varphi(z,s = (f + 1)/2)$ and $\varphi(z,s = 1)$ for folded smectic-A (fA) phases under $\beta = 10$, $\mu N = 90$ and $\chi N = 0$. (a) $f = 0.4$ and $D = 3.4R_g$; (b) $f = 0.5$ and $D = 5.0R_g$.

the coil, similar to the case of bA occurring at weak-segregation in Fig. 1(a). Folded rod-like blocks will maintain the same packing density while providing larger interfacial area, thus releasing the coil stretching frustration. Besides the observation of the fA phase, a folded smectic-C (fC) phase appears for $\beta = 10$ at high f, in which the rod-like blocks fold and also tilt an angle to the lamellar normal direction. To our knowledge, the occurrence of the fC phase has not been observed in previous theoretical and experimental studies on rod-coil systems.

Conclusions

In this work a hybrid numerical approach to solve the SCFT equations of a wormlike chain model has been developed. In this approach, the spatial-dependent functions in the theory are expanded in terms of a series of orthonormal eigenfunctions. The spectral-method restricts the solutions to a particular symmetry, thus greatly improving the numerical efficiency and accuracy. The diblock copolymers are modeled by a wormlike chain connected to a Gaussian chain, and the orientational interaction between the rod-like segments and the repulsive interaction between the different blocks are described by Maier–Saupe and Flory–Huggins interactions, respectively. As a first application of this method, one-dimensional ordered phases of semiflexible-coil diblock copolymer melts have been examined and corresponding phase diagrams have been constructed. Comparing with our previous study,[17] the current work presents new developments in methodology and phase behavior of semiflexible-coil diblock copolymers.

In contrast to the corresponding coil-coil diblock copolymers, the phase behavior and ordered morphologies of the rod-coil block copolymers depend on the coil composition f, the block repulsion characterized by χN, the Maier–Saupe orientational interaction μN, and the size asymmetry parameter β between the rods and coils. In order to focus on the two main parameters, μ/χ and β, on the phase behavior of the system, phase diagrams as a function of f and χN are constructed. A variety of smectic microstructures are found to exist in the system. A few generic features of the phase behavior can be obtained from these phase diagrams. First of all, the rod-coil repulsion, characterized by the Flory-Huggins interaction parameter χN, usually promotes the formation of smectic structures with a narrow nematic region just above the ODT. The interplay between microphase separation and orientational interaction characterized by the ratio μ/χ influences the competition between rod-coil interfacial energy and coil-stretching entropy, which plays an important role in the ordered microstructures including smectic-A, smectic-C with monolayered and bilayered rods. Therefore, a bilayer smectic-A (bA) at weak-segregation and a bilayer smectic-C (bC) structure at strong-segregation corresponding to large and small μ/χ are observed respectively. These phases were observed in experimental systems but previous theoretical simulations completely rigid rods have not been able to predict them. Secondly, we have utilized the Maier–Saupe interaction to model the ordering effects with the rod orientation denoted by **u** on a unit sphere in a 3D Euclidean space. To the best of our knowledge, this is the first time various smectic structures for a system with Maier–Saupe interactions μN and in the absence of block–block repulsion, i.e., $\chi N = 0$, have been predicted. In this case, the nematic region is observed to occupy a larger area, in contrast to the case with the block repulsions ($\chi N \neq 0$). In particular, a smectic microstructure with folded configuration for the rod block appears under strong orientational interactions in accordance with the observation of experiments by a polymer system with helix rods, which resembles the crystalline behavior of semiflexible polymers. Finally, the size asymmetry parameter β plays an important role in the phase behavior. In general, large β prefers monolayer and smectic-C structures, largely due to the increased interfacial area per chain in these phases, whereas small β prefers bilayer and smectic-A in order to decrease the interfacial energy. In future work, the hybrid numerical SCFT model will be extended to include two and three-dimensional structures although non-lamellar structures occupy minority region in the phase diagram of semiflexible block copolymers.

References

1 B. D. Olsen and R. A. Segalman, *Mater. Sci. Eng., R*, 2008, **62**, 37–66.
2 R. A. Segalman, B. McCulloch, S. Kirmayer and J. J. Urban, *Macromolecules*, 2009, **42**, 9205–9216.
3 J. T. Chen, E. L. Thomas, C. K. Ober and S. S. Hwang, *Macromolecules*, 1995, **28**, 1688–1697.
4 J. T. Chen, E. L. Thomas, C. K. Ober and G. P. Mao, *Science*, 1996, **273**, 343–346.
5 K. K. Tenneti, X. F. Chen, C. Y. Li, Y. F. Tu, X. H. Wan, Q. F. Zhou, I. Sics and B. S. Hsiao, *J. Am. Chem. Soc.*, 2005, **127**, 15481–15490.
6 A. Douy and B. Gallot, *Makromol. Chem.*, 1977, **178**, 1595–1604.
7 J. P. Billot, A. Douy and B. Gallot, *Makromol. Chem.*, 1976, **177**, 1889–1893.
8 J. P. Billot, A. Douy and B. Gallot, *Makromol. Chem.*, 1977, **178**, 1641–1650.
9 A. Douy and B. Gallot, *Polymer*, 1982, **23**, 1039–1044.
10 A. Douy and B. Gallot, *Polymer*, 1987, **28**, 147–154.
11 B. Gallot, *Prog. Polym. Sci.*, 1996, **21**, 1035–1088.
12 B. D. Olsen and R. A. Segalman, *Macromolecules*, 2007, **40**, 6922–6929.
13 B. D. Olsen and R. A. Segalman, *Macromolecules*, 2006, **39**, 7078–7083.
14 B. D. Olsen and R. A. Segalman, *Macromolecules*, 2005, **38**, 10127–10137.
15 B. D. Olsen, M. Shah, V. Ganesan and R. A. Segalman, *Macromolecules*, 2008, **41**, 6809–6817.
16 N. Sary, C. Brochon, G. Hadziioannou and R. Mezzenga, *Eur. Phys. J. E*, 2007, **24**, 379–384.
17 W. D. Song, P. Tang, H. D. Zhang, Y. L. Yang and A. C. Shi, *Macromolecules*, 2009, **42**, 6300–6309.
18 M. W. Matsen, *J. Chem. Phys.*, 1996, **104**, 7758–7764.
19 L. Onsager, *Ann. N. Y. Acad. Sci.*, 1949, **51**, 627–659.
20 W. Maier and A. Saupe, *Z. Naturforsch. A*, 1958, **13**, 564–566.
21 W. Maier and A. Saupe, *Z. Naturforsch. A*, 1959, **14**, 882–889.
22 W. Maier and A. Saupe, *Z. Naturforsch. A*, 1960, **15**, 287–292.
23 P. R. Netz and M. Schick, *Phys. Rev. Lett.*, 1996, **77**, 302–305.
24 D. Duchs and D. E. Sullivan, *J. Phys.: Condens. Matter*, 2002, **14**, 12189–12202.
25 M. Shah and V. Ganesan, *J. Chem. Phys.*, 2009, **130**, 054904.
26 M. Reenders and G. ten Brinke, *Macromolecules*, 2002, **35**, 3266–3280.

27 M. W. Matsen and C. Barrett, *J. Chem. Phys.*, 1998, **109**, 4108–4118.
28 V. Pryamitsyn and V. Ganesan, *J. Chem. Phys.*, 2004, **120**, 5824–5838.
29 M. W. Matsen and M. Schick, *Phys. Rev. Lett.*, 1994, **72**, 2660–2663.
30 F. Drolet and G. H. Fredrickson, *Phys. Rev. Lett.*, 1999, **83**, 4317–4320.
31 G. Tzeremes, K. O. Rasmussen, T. Lookman and A. Saxena, *Phys. Rev. E: Stat. Phys., Plasmas, Fluids, Relat. Interdiscip. Top.*, 2002, **65**, 041804.
32 A. Halperin, *Europhys. Lett.*, 1989, **10**, 549–553.
33 A. N. Semenov, *Mol. Cryst. Liq. Cryst.*, 1991, **209**, 191–199.
34 B. Perly, A. Douy and B. Gallot, *Makromol. Chem.*, 1976, **177**, 2569–2589.